JOURNAL OF MATERIALS SCIENCE 33 (1998) 4491–4501

# Mechanical properties of injection moulded styrene maleic anhydride (SMA)

## Part II *Influence of short glass fibres and weldlines*

A. CHRYSOSTOMOU, S. HASHEMI
*School of Polymer Technology, University of North London, Holloway Road, London N7 8DB, UK*
*E-mail: s.hashemi@unl.ac.uk*

The dependence of the various mechanical and fracture properties on the volume fraction of short glass fibres in the styrene maleic anhydride (SMA) polymer was investigated. Special attention has been given to describing the dependence of various mechanical properties on the volume fraction of the glass fibres, $\phi_f$ by way of the rule of mixtures. It was found that, strength, elastic modulus and fracture toughness, all follow a simple rule-of-mixtures of the form $Q_c = \lambda Q_f \phi_f + Q_m(1 - \phi_f)$, where $Q_c$ is the measured quantity for the composite, $Q_m$ and $Q_f$ are the corresponding values for the matrix and the fibre, respectively, and $\lambda$ is the overall efficiency of the fibres, taking into account the orientation and the length of the fibres in the composite. It was also found that, while the presence of the weldline had no significant effect upon elastic modulus, its presence significantly reduced tensile strength and the fracture toughness of SMA and its composites. 

## 1. Introduction

Incorporating short fibres into polymer matrices has received considerable attention because of their use in a variety of engineering applications. It has been well established that the mechanical properties (e.g. strength and modulus) of the polymer matrix are enhanced by the addition of the short fibres. These properties, however, are affected by a number of parameters, such as volume fraction of fibres, fibre length, fibre orientation and the degree of interfacial adhesion between fibre and matrix. It has been shown (e.g. [1–8]) that the dependence of most mechanical properties on the volume fraction of the fibres my be described using some modified form of the rule of mixtures, which considers both the orientation of the fibres and distribution of fibre lengths in the composite.

As most short-fibre composites are fabricated by injection moulding, weldlines can often be seen on the moluded component when two flowing polymer fronts are brought into contact. The presence of such moulding defects can cause deterioration in mechanical properties, particularly in short-fibre composite systems where fibres at the weldline may assume an orientation which is perpendicular to the direction of the applied stress.

In Part 1 of this paper [8], we investigated the effects of reprocessing and weldlines on deformation and fracture properties of SMA polymer. In this paper, we report the effects of short glass fibres and weldliness on the deformation and fracture behaviour of injection-moulded styrene maleic anhydride (SMA) polymer.

## 2. Experimental procedure

### 2.1. Materials

The styrene maleic anhydride material used is commercially available under the trade name "Strapton SMA 400" manufactured by DSM. In addition to the neat matrix, the following SMA composites containing different amounts of short glass fibres were also received:

(i) SMA 400 reinforced with 20 wt % short glass fibres (SMA 440);
(ii) SMA 400 reinforced with 30 wt % short glass fibres (SMA 460);
(iii) SMA 400 reinforced with 40 wt % short glass fibres (SMA 480);

All the materials were received in granular form and dried prior to injection moluding for 3 h at 90 °C as recommended by the manufacturer.

### 2.2. Mouldings

Dumb-bell-shaped specimens of dimensions 12.5 mm × 1.7 mm × 125 mm (thickness, depth, length) were produced on a Negri Bossi NB60 using the processing conditions given in Table I. The mould used was consisted of two cavities, a single and a double feed cavity as shown in Fig. 1. In the latter,

TABLE I Processing conditions

| | SMA400 | SMA440 | SMA460 | SMA480 |
|---|---|---|---|---|
| Barrel temperature (°C) | | | | |
| Zone 1 | 235 | 240 | 240 | 240 |
| Zone 2 | 240 | 245 | 245 | 245 |
| Zone 3 | 240 | 245 | 245 | 245 |
| Mould temperature (°C) | 80 | 80 | 80 | 80 |
| Pressure (MPa) | 75 | 110 | 110 | 110 |
| Hold pressure (MPa) | 45 | 55 | 55 | 55 |
| Injection speed (mm $s^{-1}$) | 31 | 35 | 35 | 35 |
| Injection time (s) | 9 | 9 | 9 | 9 |
| Cooling time (s) | 30 | 30 | 30 | 30 |

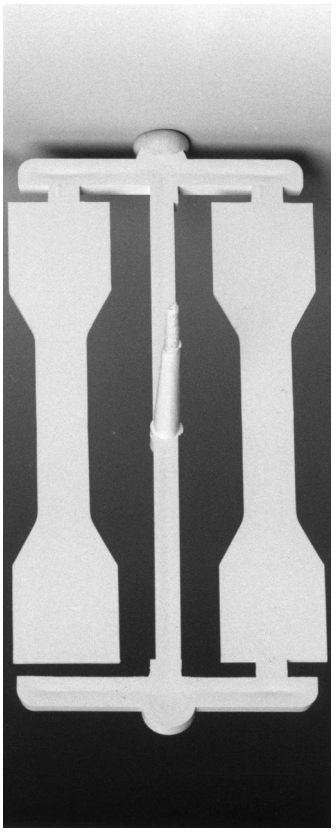

*Figure 1* Moulding test pieces.

a weldline is formed mid-way along the gauge length as the two opposing melt fronts meet.

## 2.3. Sample characterization

### *2.3.1. Fibre concentration measurements*

The fibre concentration in each composite was determined by ashing the material. A suitable amount of material was weighed accurately and then placed in a furnace at 550 °C for at least 1 h. After cooling, the remnant was reweighed and the weight fraction of the fibres was determined, $w_f$. It was found that the measured weight fractions were within 1% of the manufacturer's specification.

From the knowledge of the fibre and matrix densities, the volume fraction of the fibres, $\phi_f$, in each composite was calculated using the following relationship:

$$\phi_f = \left[1 + \frac{\rho_f}{\rho_m}\left(\frac{1}{w_f} - 1\right)\right]^{-1} \quad (1)$$

where $\rho_m$ is the density of the matrix ($= 1.10$ g $cm^{-3}$) and $\rho_f$ is the density of the glass fibre ($= 2.54$ g $cm^{-3}$).

### *2.3.2. Fibre length measurements*

The same ashing experiment was carried out with the injection-moulded specimens in order to determine the average length of the fibre in each composite. The ash for each composite was spread on a glass slide and then placed under a light optical microscope and photographed. At least 300–400 fibre lengths were measured for each composite and a frequency distribution of the fibre lengths was plotted (see Fig. 2), from which the number average fibre length, $L_f$, was determined. The average length of the fibre was found to be 224 μm for SMA 440, 231 μm for SMA460 and 248 μm for SMA480.

### *2.3.3. Fibre orientation*

Fibre orientation distributions were studied using polished specimens. The polished surfaces were then viewed under an optical light microscope and photographed.

## 2.4. Mechanical testing

### *2.4.1. Tensile and flexural properties*

Elastic modulus and strength of the SMA polymer and its composites were measured in both tension and three-point flexure using an Instron testing machine.

Tensile tests were performed on dumb-bell specimens at a crosshead displacement rate of 5 mm $min^{-1}$ using pneumatic clamps. From the recorded load–displacement curves, values of tensile strength and modulus were calculated using the maximum load and the initial slope, respectively.

Measurements of flexural strength and modulus were made on rectangular strips of nominal dimensions 12.5 mm × 1.7 mm × 50 mm (thickness, width, length), cut from the parallel portion of the unwelded dumb-bell specimens. Strips were then tested in three-point bend configuration (see Fig. 3) at a crosshead displacement rate of 5 mm $min^{-1}$ using a span width of 28 mm (i.e. span to depth ratio of 16:1). From the recorded load–displacement curves, values of flexural strength and modulus were calculated using the

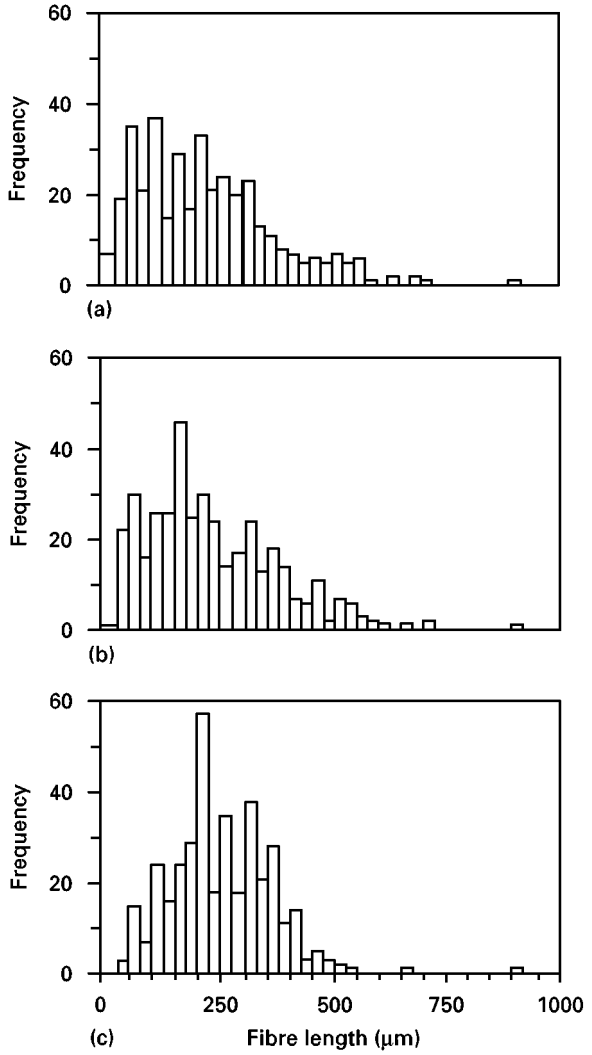


*Figure 2* Fibre length distributions: (a) SMA 440, (b) SMA 460, (c) SMA 480.

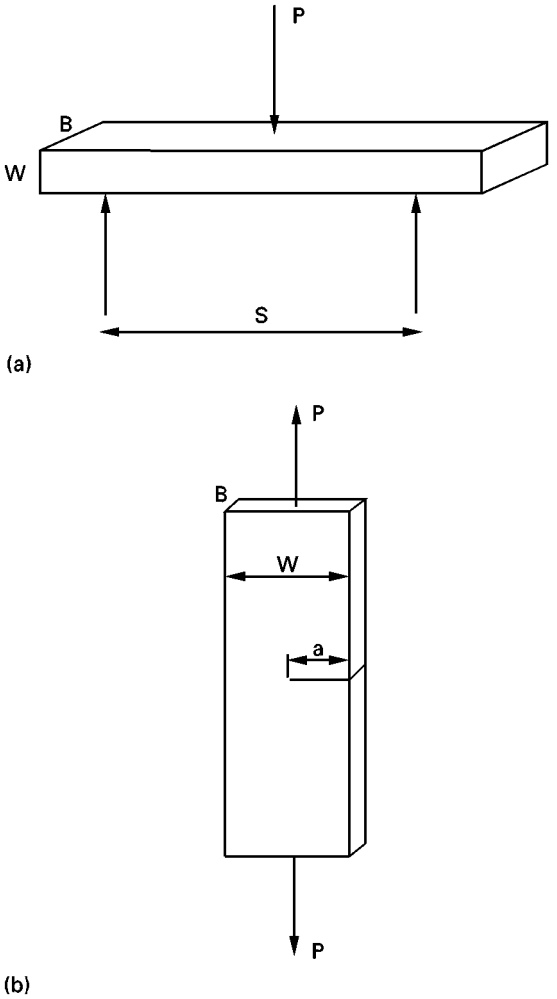


*Figure 3* Test specimens: (a) flexural specimen, (b) single-edge notched tension specimen.

following linear elastic beam equations

$$E = \frac{1}{4B}\left(\frac{P}{\delta}\right)_0\left(\frac{S}{W}\right)^3 \tag{2}$$

$$\sigma_{max} = \frac{3P_{max}S}{2BW^2} \tag{3}$$

where $P_{max}$ and $(P/\delta)_0$ are the maximum load and the initial slope of the load–displacement diagram, respectively. $B$ and $W$ are the thickness and the width of the specimen, respectively, and $S$ is the span width.

### 2.4.2. Dynamic mechanical analysis (DMA)

Dynamic tests for determination of storage modulus were performed on a Perkin–Elmer 7 series. These tests were performed on rectangular strips of dimensions 4 mm × 1.7 mm × 17 mm (thickness × depth × length) also cut from the parallel portion of the unwelded dumb-bell specimens. Strips were tested in three-point bend configuration over a span of 15 mm (i.e. span to depth ratio of 8.82). Tests were performed at a frequency of 1 HZ, dynamic force of 400 mN and a static force of 600 mN. The temperature range over which testing was conducted was between 30 and 130 °C using increments of 5 °C min$^{-1}$.

### 2.4.3. Fracture toughness

Fracture toughness of the SMA polymer and its composites was measured in tension using single-edge notched specimens (see Fig. 3). Rectangular strips of nominal dimensions of 1.7 mm × 12.5 mm × 70 mm (thickness, $B$ × depth, $D$ × length) were cut from the parallel portion of both welded and unwelded dumb-well specimens and then edge notched to various $a/W$ ratios ($a$ = crack length) ranging from 0.1–0.6 using a razor blade. The blade was mounted on a purpose-made device to make sure that it was precisely and perpendicularly guided through the cross-section of the specimen. In the case of specimens with weldlines, care was taken to ensure that the initial notch was inside the weldline. After notching, each specimen was tested to complete failure in an Instron testing machine at a constant crosshead displacement rate of 5 mm min$^{-1}$ using pneumatic clamps with a gauge length of 50 mm. A load–displacement curve for each specimen was recorded for subsequent analysis.

## 3. Results and discussion

### 3.1. Deformation behaviour of single-gated mouldings

#### *3.1.1. Elastic modulus*

According to the load–displacement curves in Fig. 4a, deformation of SMA and its composites during the early stages of the tests in both tension and flexure was linearly elastic. Using the initial slope of the curves, values of the elastic modulus in both tension and flexure were calculated and plotted as a function of fibre concentration as shown in Fig. 5. It is seen that the elastic modulus increases linearly with increasing fibre concentration and that for a given fibre concentration value, flexural modulus is considerably higher than tensile modulus.

In the calculation of tensile modulus, we assumed that the displacement of the specimen is the same as the sepration of the clamps. Previous studies have shown that such an assumption could lead to a modulus value which is lower than the actual modulus of the material as a result of machine compliance, gear train, etc. However, if the additivity of strains in the sample and the instrument is assumed, then the actual modulus, $E_{act}$, can be obtained via the following relationship [3]

$$\frac{1}{E_{app}} = \frac{1}{E_{act}} + k\frac{A}{Z} \tag{4}$$

where $E_{app}$ is the apparent modulus (the measured value), $Z$ and $A$ are the gauge length and the cross-sectional area of the specimen, respectively, and $k$ is an instrument constant. According to Equation 4 the actual modulus can be ascertained from the inverse of the intercept at $A/Z = 0$ of a linear regression line interpolating the plot of $1/E_{app}$ versus $A/Z$. Such a plot was constructed for SMA and its composites as shown in Fig. 6, by varying the gauge length, $Z$, but keeping the cross-sectional area, $A$, constant. The inverse of the intercept values at $A/Z = 0$ are plotted in Fig. 5, where it can be seen, that the corrected values of tensile modulus, $E_{act}$, agree quite well with the flexural values.

#### *3.1.2. Analysis of elastic modulus*

The most commonly used theory to model the variation of the composite stiffness as a function of the fibre concentration is that of the Cox "shear lag" model [1]. This model is based on the assumption that discontinuous fibres are aligned in the direction of the applied stress and that the applied stress is transferred from the matrix to the fibres via interfacial shear stresses, with the maximum shear occurring at the fibre ends and decreasing to zero at the centre.

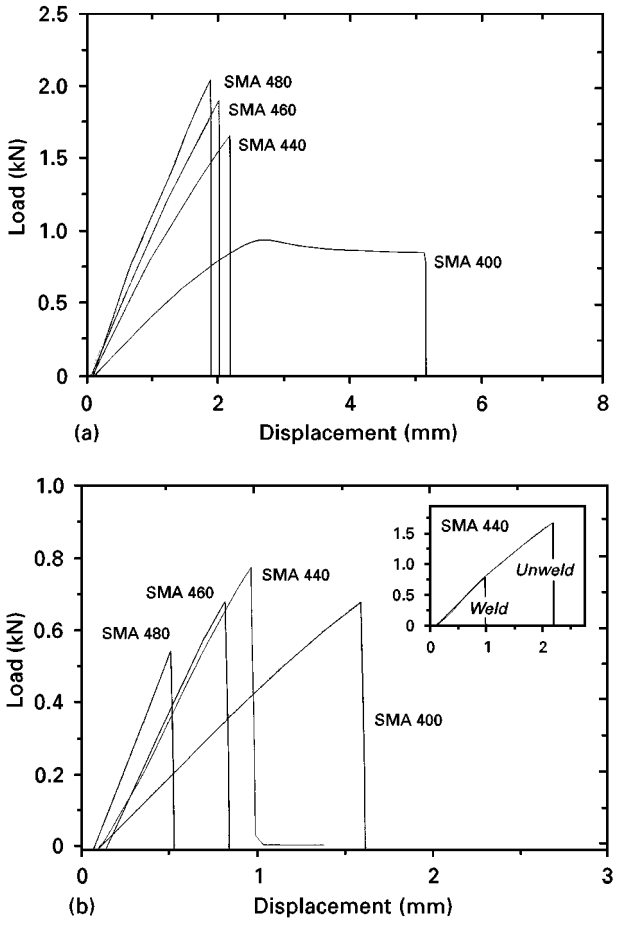


*Figure 4* Tensile load–displacement diagrams for SMA and its composites. (a) Unwelded, (b) welded.

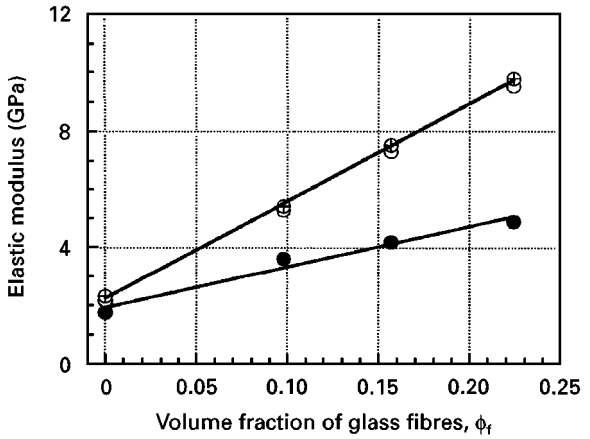


*Figure 5* (●) Tensile and (○) flexural modulus versus volume fraction of glass fibres. (⊕) $E_{act}$.

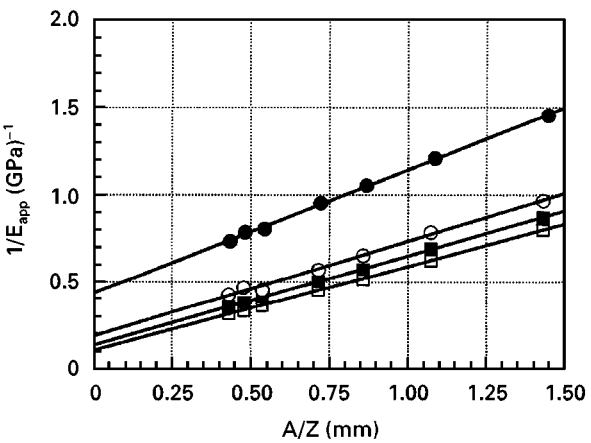


*Figure 6* $1/E_{app}$ versus $A/Z$ for tensile tests: SMA (●) 400, (○) 440, (■) 460, (□) 480.

Consequently, the tensile stress in the fibre is zero at its ends and reaching a maximum half way along its length. Although the efficiency of stress transfer increases with increasing fibre length, it can never reach 100%. In order to accommodate this dependence of reinforcement efficiency on fibre length, Cox introduced a fibre length efficiency factor, $\chi_1$, into the "rule-of-mixtures" for the composite modulus, $E_c$

$$E_c = \chi_1 E_f \phi_f + E_m(1 - \phi_f) \quad (5)$$

where $E_f$ and $E_m$ are the elastic moduli of the fibre and the matrix, respectively. The "shear lag" theory defines $\chi_1$ as

$$\chi_1 = 1 - \frac{\tanh \beta L/2}{\beta L/2} \quad (6)$$

where $L$ is the average fibre length, and $\beta$ is defined as

$$\beta = \left[ \frac{\pi E_m}{(1 + \nu_m) E_f A_f \ln (R/r)} \right]^{1/2} \quad (7)$$

where $\nu_m$ is Poisson's ratio of the matrix, $r$ is the radius of the fibre, $A_f$ is the cross-sectional area of the fibre and $2R$ is the interfibre spacing. For an assumed square packing arrangement of fibres with volume fraction $\phi_f$, the following substitution can be made

$$R = r\left( \frac{\pi}{4\,\phi_f} \right)^{1/2} \quad (8)$$

Krenchel [9] modified Equation 5 in order to take into account the contributions to the modulus from the misaligned fibres. The contribution was allowed for by incorporating a fibre orientation factor, $\chi_2$, into Equation 5

$$E_c = \chi_1 \chi_2 E_1 \phi_f + E_m(1 - \phi_f) \quad (9)$$

where for aligned-longitudinal orientation $\chi_2 = 1$, for aligned-transverse $\chi_2 = 0$ and for random-in-plane orientation of the fibres $\chi_2 = 0.375$.

For our purposes we write Equation 9 as

$$E_c = E_m + (\chi_E E_f - E_m)\phi_f \quad (10)$$

where $\chi_E$ represents the overall fibre efficiency parameter for the modulus ($= \chi_1 \chi_2$). From the data in Fig. 5 we obtain

$$E_c = 2.26 + 33.47\,\phi_f \quad (r^2 = 0.998) \quad (11)$$

thus giving a $\chi_E$ value of 0.476 for an $E_f$ value of 75 GPa. The fibre length efficiency parameter, $\chi_1$, for each composite was calculated using Equations 6–8 (taking $\nu_m = 0.35$ and $r = 5\ \mu m$), and the corresponding value of the orientation efficiency parameter was then estimated as $\chi_2 = \chi_E/\chi_1$. It is seen from Table II that the efficiency parameters do not change significantly with $\phi_f$ and that estimated values of $\chi_2$ are much higher than 0.375, expected for random-in-plane orientation of fibres. Indeed, according to optical micrographs in Fig. 7, fibres throughout the cross-section of the specimens have high degree of alignment with no apparent change in the orientation patterns as one moves from the surface of the specimen (skin) to its centre (i.e. core). Using Krenchel's [9] definition of $\chi_2$

$$\chi_2 = \sum_{i=1}^{i=n} a_n \cos^4 \theta_n \quad (12)$$

and assuming perfect alignment of fibres (i.e. $a_n = 1$), we find that a $\chi_2$ value of 0.644 corresponds to a fibre orientation angle, $\theta$ (with respect to the direction of the applied stress which is also the mould-fill direction), of approximately 26°.

TABLE II Efficiency parameters

| | | $\chi_E = 0.476$ | | $\chi_S = 0.142$ | |
|---|---|---|---|---|---|
| $\phi_f$ | $L_f$ | $\chi_1$ | $\chi_2$ | $\chi_3$ | $\chi_4$ |
| 0.098 | 224 | 0.696 | 0.684 | 0.22 | 0.645 |
| 0.157 | 231 | 0.740 | 0.643 | 0.23 | 0.617 |
| 0.224 | 248 | 0.786 | 0.605 | 0.24 | 0.592 |

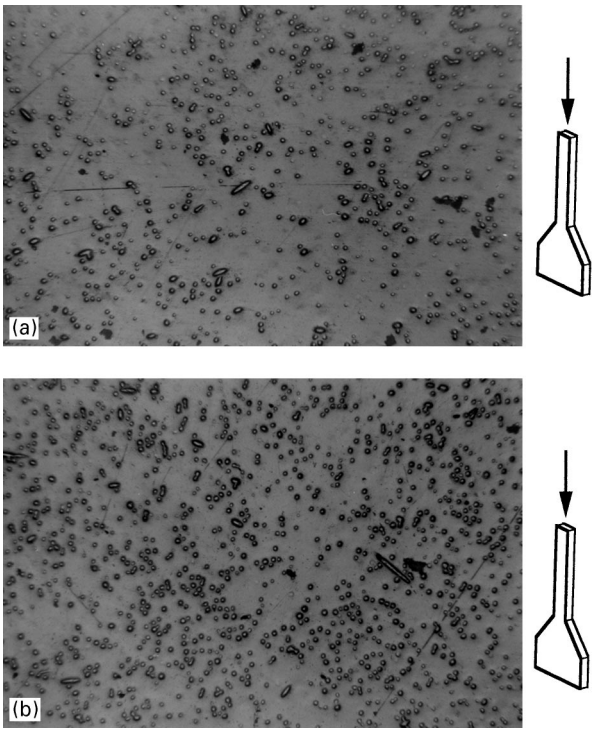


*Figure 7* Optical micrographs showing fibre orientation in SMA 460 and SMA 480 unwelded tensile specimens. (Flow direction is normal to the paper.) (a) $\phi_f = 15.7\%$, (b) $\phi_f = 22.4\%$.

### 3.1.3. Strength

It is seen from the load–displacement displacement diagrams (Fig. 4a) that the matrix material shows lower strength but higher extension to failure compared to its composites. This is expected, because tri-axial restraint of the matrix between the fibres limits the elongation of the matrix and thereby reduces its elongation to failure. It was noted that, whereas failure of all SMA specimens in tension and in flexure was ductile in so far as the point of fracture occurred after the yield point, that of the glass-reinforced SMA specimens was brittle.

The dependence of tensile and flexural strengths on volume fraction of glass fibres is shown in Fig. 8 where it can be seen that the dependence is linear for values of $\phi_f$ less than 22%. Seemingly, close to this volume fraction, the separation distance between the fibres has become sufficiently small to restrict the flow of the matrix material and to reduce the gain in strength which was otherwise expected with increasing $\phi_f$.

It is seen from Fig. 8 that, as in the case of elastic modulus, the strength of the unfilled and filled SMA materials in flexure is considerably higher than in tension. However, the correction applied to tensile modulus does not apply to tensile strength, as in this case one needs to know only the load and the area, but not the strain. It is well established, however, that in tensile test, the whole volume of the specimen is subjected to a uniform state of tensile stress, whereas in the flexure test due to non-uniformity of stress distribution, tensile stress decreases from a maximum value at the surface to a zero volue at the neutral axis. The measured strength by way of the tensile test thus indicates a mean value of stress across the specimen thickness as opposed to the maximum value calculated in flexure using Equation 3. It is worth noting that, when data in Fig. 8 are plotted as relative strength (i.e. strength of the composite divided by that of the matrix) versus $\phi_f$, as in Fig. 9, the loading mode effect becomes very insignificant.

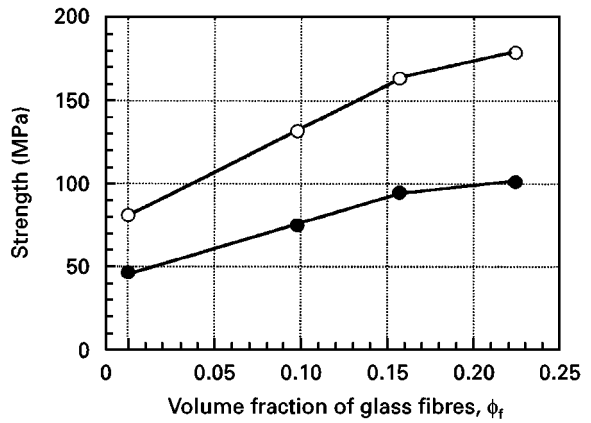


*Figure 8* Tensile and flexural strengths versus volume fraction of glass fibres.

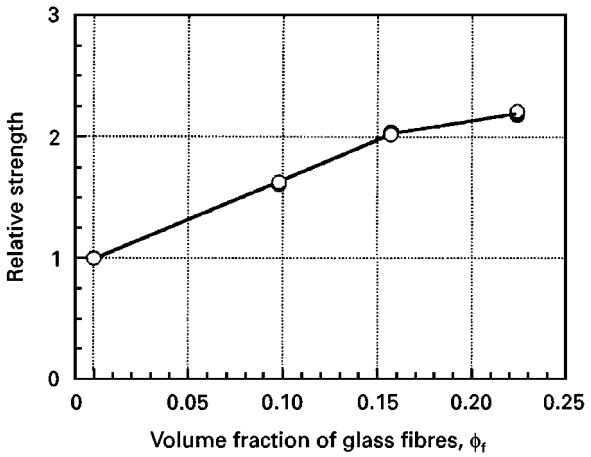


*Figure 9* Relative strengths versus volume fraction of glass fibres. (○) flexural, (●) tensile.

### 3.1.4. Analysis of tensile and flexural strengths

The linearity of the tensile and flexural strengths with $\phi_f$ suggested that these quantities, like elastic modulus, may obey some form of rule-of-mixtures. It has been shown by Kelly and Tyson [2], that the strength of short-fibre composites, $\sigma_c$, may be related to the volume fraction of fibres by the following rule-of-mixtures

$$\sigma_c = \chi_3 \chi_4 \sigma_f + \sigma_m(1 - \phi_f) \tag{13}$$

where $\sigma_f$ and $\sigma_m$ are tensile strengths of the fibre and the matrix, respectively, and parameters $\chi_3$ and $\chi_4$ are the fibre length and fibre orientation efficiency factors, respectively. Equation 13 can be written as

$$\sigma_r = 1 + \left( \chi_S \frac{\sigma_f}{\sigma_m} - 1 \right) \phi_f \tag{14}$$

where $\sigma_r = \sigma_c/\sigma_m$ and $\chi_S$ is defined as the overall fibre efficiency parameter for strength ($\chi_S = \chi_3\chi_4$).

According to Kelly and Tyson [2], the value of $\chi_3$ depends on whether the average length of the fibre in the specimen is supercritical or subcritical, the critical length, $L_c$, being given as

$$L_c = \frac{d\sigma_f}{2\tau_i} \tag{15}$$

where $\tau_i$ is the shear strength of the interface. For the case in which $L < L_c$, $\chi_3$ may be calculated from

$$\chi_3 = \frac{L_f}{2L_c} \tag{16}$$

and for the case in which $L > L_c$, from

$$\chi_3 = 1 - \frac{L_f}{2L_c} \tag{17}$$

The critical fibre length was measured to be 510 μm, which is almost twice the average length of the fibre. Consequently, $\chi_3$ for each composite was calculated using Equation 16; values can be found in Table II. The best linear regression line fitted through the data in Fig. 9 for values of $\phi_f$ less than 0.22 gave the following relationship between the relative strength and the volume fraction of glass fibres

$$\sigma_r = 1 + 6.54\,\phi_f \tag{18}$$

Comparing Equations 18 and 14, one obtains a $\chi_S$ value of 0.142 (taking $\sigma_f$ as 2470 MPa and $\sigma_m$ as 46.48 MPa), thus giving $\chi_4$ values ranging from 0.59–0.65 ($\chi_4 = \chi_S/\chi_3$).

It can be seen from Table II, that values of the orientation efficiency parameters $\chi_2$ and $\chi_4$ agree quite well as one might expect because the data for modulus and strength were obtained from the same mouldings. The idea of using modified rule-of-mixtures to describe the dependence of modulus and strength on $\phi_f$, thus seems appropriate.

## 3.2. Deformation behaviour of double-gated mouldings

### *3.2.1. Elastic modulus*

The deformation behaviour of the SMA and its composites in the elastic region was only marginally affected by the presence of the weldline (see the insert in Fig. 4b). The weldline integrity parameter for modulus, defined as the ratio of the modulus of a specimen with a weldline to that of an identical specimen without a weldline, ranged between 1.0 and 0.97, thus indicating that the presence of the weldline has little effect, if any, on tensile modulus. This behaviour was interpreted by the model used by Nabi and Hashemi [7] to explain the insensitivity of the tensile modulus to weldlines in glass fibre-reinforced ASA copolymer. The model predicts that modulus of a tensile specimen with a weldline, $E_w$, may be related to the modulus of the material inside and outside the weldline ($E_1$ and $E_2$, respectiely) by the following relationship

$$E_w = \frac{E_1 E_2}{E_2 + (E_1 - E_2)z} \tag{19}$$

where $z$ is the ratio of the weldline width to specimen gauge length. Because $z$ is very small for SMA and its composites (typically less than 1 mm), the second term in the denominator is small compared to $E_2$ thus indicating that $E_w \approx E_2$ as observed here.

### *3.2.2. Tensile strength*

Tensile failure of all weldline specimens was brittle as shown in Fig. 4b and it occurred at the weldline. It can be seen from Fig. 4a and b that double-gated specimens fracture at a significantly lower stresses than their respective single-gated specimens. In the case of SMA, the observed reduction in tensile strength in the presence of the weldline was attributed mainly to the reduction in the fraction of the polymer chain molecules crossing the weldline region (i.e. parallel to the direction of the applied stress). For composites, the observed reduction in tensile strength in the pressence of the weldline was attributed mainly to the reduction in the fraction of the fibres crossing the weldline region, particularly at high concentration values of glass fibres. As a result, the material within the weldline region acted as if it was not reinforced. This is supported by the optical micrographs shown in Figs 10 and 11 where it can be seen that the majority of glass fibres in the weldline region tend to align themselves in a direction which is more or less parallel to the weldline surface, i.e. perpendicular to the direction of the applied tensile force. Away from the weldline region, fibres do tend to assume an orientation which is similar to that observed in single-gated specimens.

It is seen from Fig. 12, that the presence of glass fibres could either have a positive or a negative effect upon weldline strength, depending on the volume fraction of the glass fibres present in the specimen. Seemingly, below a certain volume fraction of fibres, say $\phi_c$, weldline strength increases with increasing $\phi_f$, whereas above this volume fraction it decreases with increasing $\phi_f$. According to the data, the decrease in

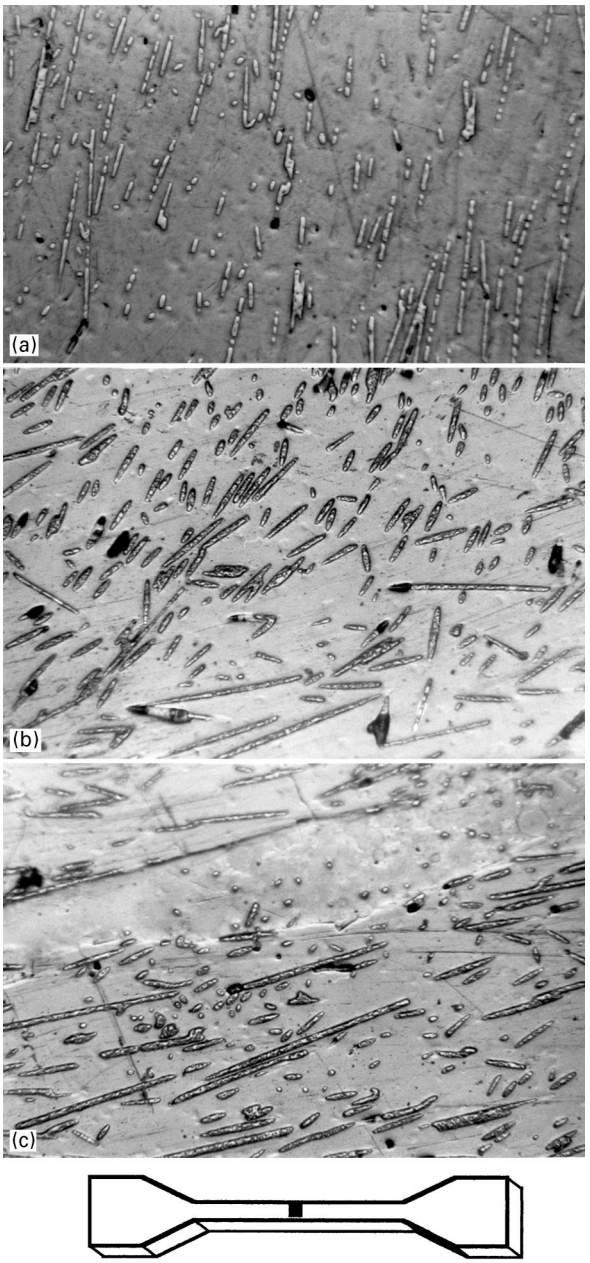


*Figure 10* (a–c) Optical micrographs showing fibre orientation inside and outside of the weldline region in SMA 480. (Flow directions are parallel to the plane of the paper.)

weldline strength, $\sigma_{cw}$, with increasing $\phi_f$ tends to be linear, giving

$$\sigma_{cw} = 43.49 - 80.92\,\phi_f \qquad (\phi_f > \phi_c) \tag{20}$$

It is worth noting that the extrapolated value of weldline strength at $\phi_f = 0$ is not significantly lower than the unwelded tensile strength of 46.48 MPa for the matrix. It may be said that the intercepted value represents weldline strength of the matrix in the absence of the polymer chain orientation, parallel to the weldline region. The above equation may thus be written as

$$\sigma_{cw} \approx \sigma_m(1 - 1.78\,\phi_f) \qquad (\phi_f > \phi_c) \tag{21}$$

It may be postulated that for values of $\phi_f$ less than $\phi_c$, the strength of the weldline is determined mainly by the orientation of the polymer chain in the weldline region, whereas for values of $\phi_f$ greater than $\phi_c$, the

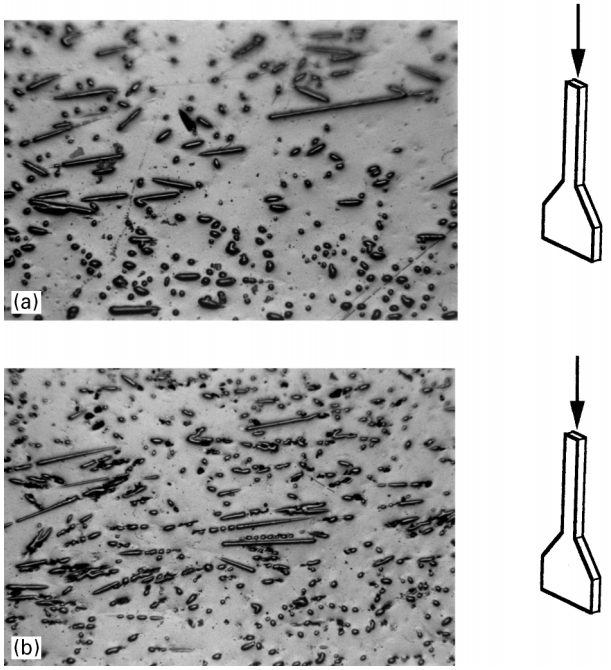


*Figure 11* Optical micrographs showing fibre orientation in weldline regions of SMA 460 and SMA 480 tensile specimens. (Flow direction is norml to the plane of the paper.) (a) $\phi_f = 15.7\%$, (b) $\phi_f = 22.4\%$.

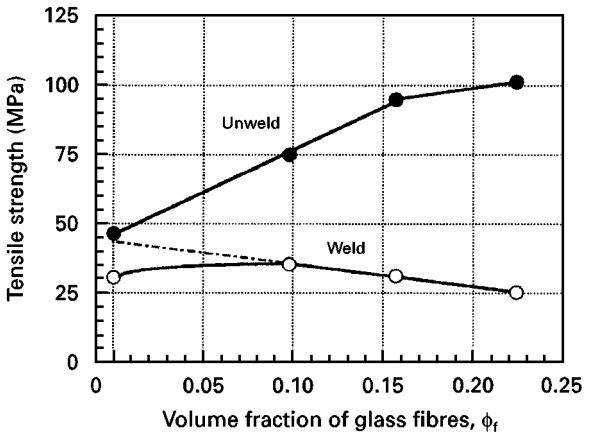


*Figure 12* Comparison between the welded and unwelded tensile strengths as a function of the volume fraction of glass fibres.

determining factor is the orientation of the fibres in the weldline region.

The effect of weldline on tensile strength is quantitatively expressed in Fig. 13 in terms of weldline integrity parameter, $F$. It is seen that $F$ decreases linearly from a value of 0.66 for the matrix to a value of 0.30 for the composite containing 15.7 vol % glass fibres. This linear dependence on $\phi_f$ can be expressed as

$$F_c = F_m(1 - \gamma\phi_f) \tag{22}$$

where $F_m$ and $F_c$ are the weldline integrity parameters for matrix strength and composite strength, respectively, and $\gamma = 3.13$. It is worth noting that a combination of Equations 14 and 22 predicts

$$\sigma_{cw} = \sigma_{mw}[1 + (\Omega - \gamma)\phi_f - \Omega\gamma\phi_f^2] \tag{23}$$

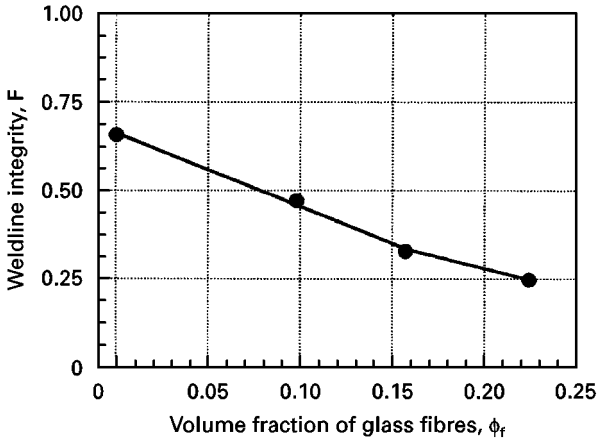


*Figure 13* Weldline integrity parameter for tensile strength versus volume fraction of glass fibres.

with a maximum at a critical fibre concentration value of

$$\phi_c = \frac{\Omega - \gamma}{2\Omega\gamma} \tag{24}$$

where $\Omega = (\chi_S\sigma_f/\sigma_m - 1)$. According to Equation 18, $\Omega = 6.54$, thus we obtain that maximum weldline strength occurs at a $\phi_c$ value of approximately 8%.

## 3.3. Dynamic testing

Fig. 14 shows typical DMA traces of storage modulus for SMA and its composites. It can be seen from Fig. 15, that the value of storage modulus in the glassy region increases with increasing $\phi_f$. Although this variation, like elastic modulus, is linear with respect to $\phi_f$, dynamic values for the three composites appear to be considerably lower than their respective static values. The solid line in Fig. 15 suggests the following relationship between storage modulus and $\phi_f$

$$E_c = 2.04 + 15.27\,\phi_f \tag{25}$$

The overall fibre efficiency parameter, $\chi_E$, in this case is 0.23 compared to a value of 0.476 obtained from the static tests. Assuming, the orientation efficiency parameter $\chi_2$ is independent of the testing conditions, we estimate a fibre length efficiency parameter, $\chi_1$, of 0.357 which is half the value obtained from the static tests.

## 3.4. Fracture of single-gated mouldings

All the single-edge notched tension specimens were fractured in unstable manner as indicated by the load–displacement diagrams in Fig. 16a. In the case of SMA, unstable failure occurred after some degree of yielding at the tip of the crack, accompanied by a small amount crack growth. As a result, load–displacement diagrams for SMA specimens exhibited some degree of non-linearity prior to attaining the maximum load as illustrated more clearly in Fig. 16b.

The concept of linear elastic fracture mechanics (LEFM) was used to determine the fracture toughness,

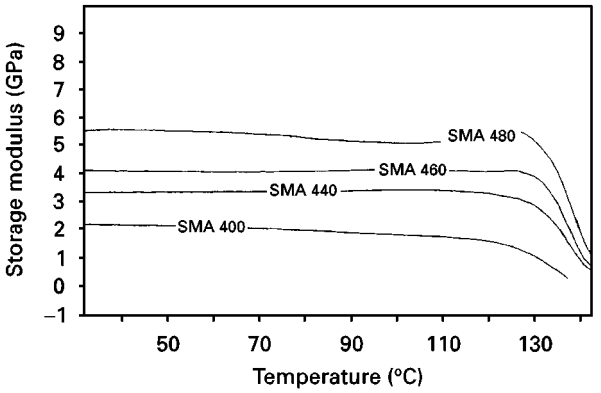


*Figure 14* DMA traces of storage modulus for SMA and its composites.

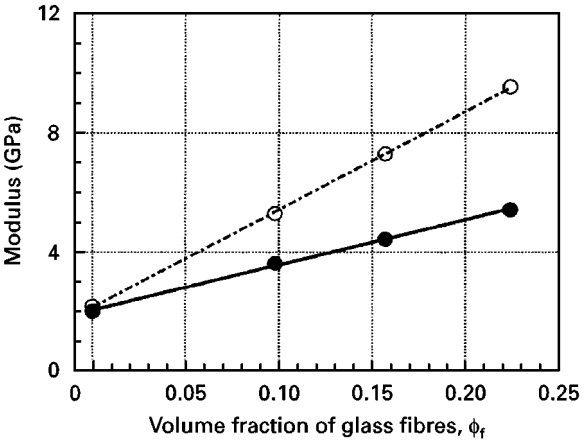


*Figure 15* (●) Storage modulus versus volume fraction of glass fibres: (○) flexural modulus.

$K_c$, of the SMA and its composites. $K_c$ was determined from the well-known linear elastic fracture mechanics relationship [10]

$$K_c = \frac{P_{max}}{BW} Y(a/W) a^{1/2} \quad (26)$$

where $P_{max}$ is the maximum load, $a$ is the initial crack length and $Y(a/W)$ is the finite width correction whose value for single-edge notched tension specimens with fixed ends can be obtained from [11]

$$Y(a/W) = \frac{5\pi^{1/2}}{[\sqrt{20 - 13(a/W) - \gamma(a/W)^2}]^{1/2}} \quad (27)$$

Fig. 17 shows plots of $\sigma_{max}$ versus $1/Ya^{1/2}$ for SMA and its composites. As can be seen, plots are reasonably linear as required by linear elastic fracture mechanics. Values of $K_c$ determined from the slope of these lines are plotted in Fig. 18a as a function of $\phi_f$, where it can be seen that $K_c$ increases with increasing $\phi_f$. It is worth noting, that the $K_c$ of the three composites, $K_{cc}$, follows a straight-line relationship with respect to $\phi_f$, defined as

$$K_{cc} = 1.80 + 16.97\ \phi_f \quad (28)$$

It is noted, that the intercept value at $\phi_f = 0$, is considerably lower than the measured value of

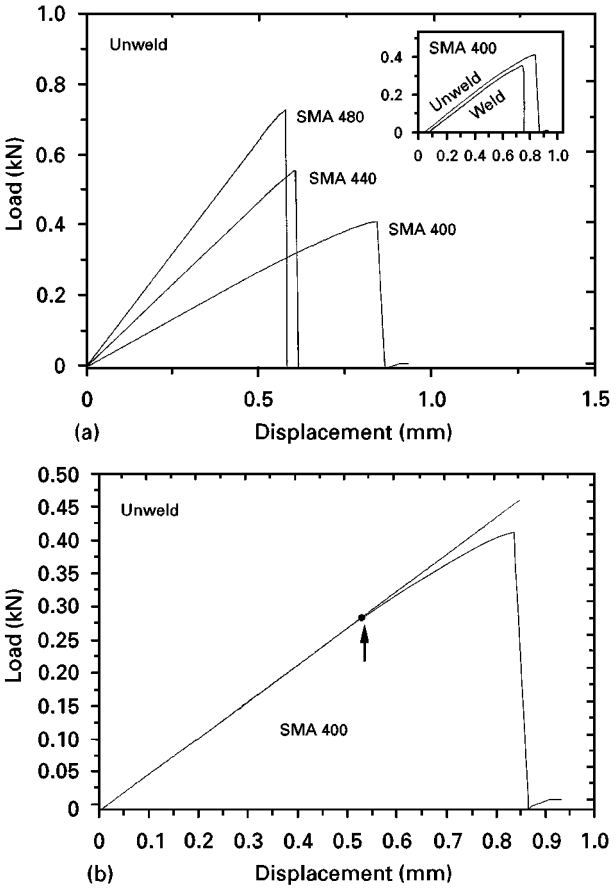


*Figure 16* Typical load–displacement diagrams for single-edge notched tension specimens without weldlines.

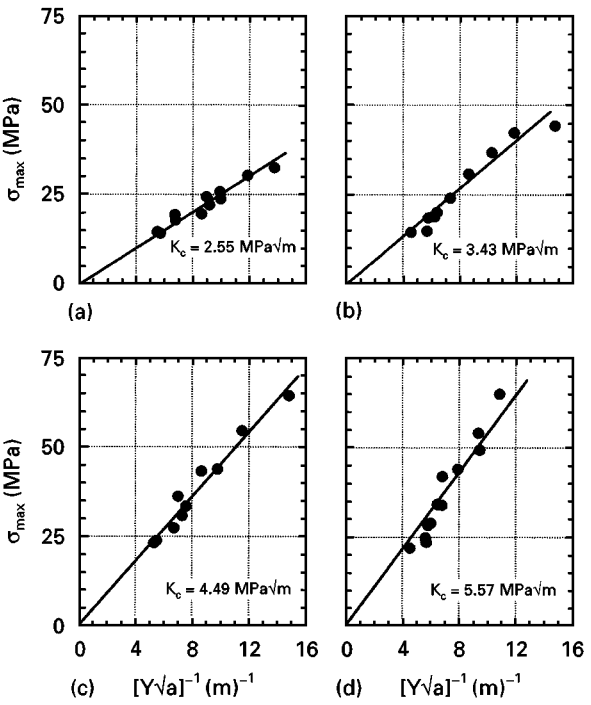


*Figure 17* Maximum stress versus $1/Ya^{1/2}$ for single-edge-notched tension specimens without weldlines: (a) SMA 400, (b) SMA 440, (c) SMA 460, (d) SMA 480.

2.55 MPa $m^{1/2}$, for the SMA. However, as shown in Fig. 16b, the load corresponding to a $K_c$ value of 1.8 MPa $m^{1/2}$, coincides more or less with the load at which the load–displacement diagram for SMA

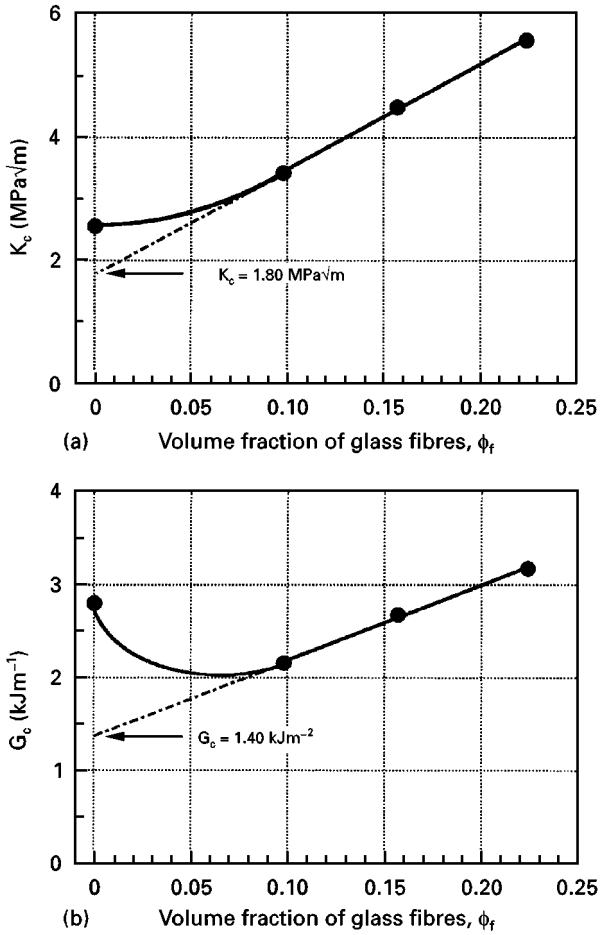


*Figure 18* (a) Fracture toughness versus volume fraction of glass fibres for specimens without weldlines. (b) Strain energy release rate for unwelded specimens versus volume fraction of glass fibres.

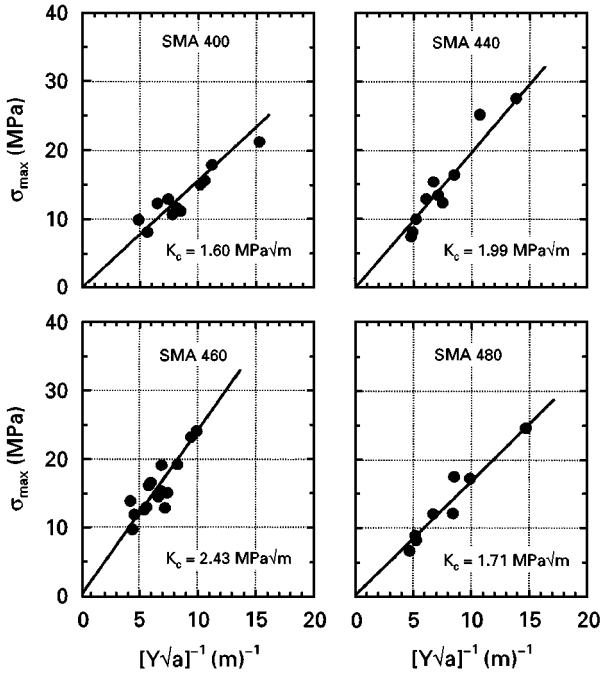


*Figure 19* Maximum stress versus $1/Ya^{1/2}$ for single-edge notched tension specimens with weldlines.

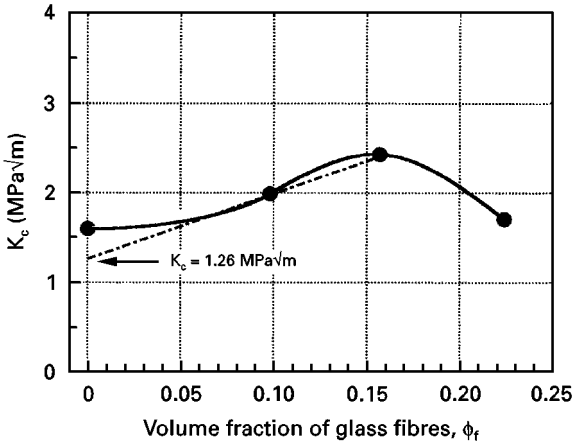


*Figure 20* Fracture toughness versus volume fraction of glass fibres for specimens with weldlines.

deviated from linearity. Visual detection of the specimens during the tests suggested that the intercept value of 1.80 MPa m$^{1/2}$, may be regarded as the initiation fracture toughness of the SMA polymer.

According to linear elastic fracture mechanics, the critical value of the strain energy release rate, $G_c$, can be calculated from the $K_c$ value via the relationship

$$G_c = \frac{K_c^2}{E} \tag{29}$$

where $E$ represents the elastic modulus of the material. The $G_c$ values calculated using the above relationship are plotted as a function of $\phi_f$ in Fig. 18b. Once again, $G_c$ of the three composites follows a linear trend which can be described as

$$G_{cc} = 1.40 + 7.97\ \phi_f \tag{30}$$

giving an initiation value of 1.4 kJ m$^{-2}$ for SMA.

## 3.4. Fracture of double-gated mouldings

All double-gated specimens fractured in an unstable manner at maximum load. In the case of SMA, load–displacement diagrams exhibited some degree of non-linearity prior to maximum load (e.g. see insert in Fig. 16a). Using the maximum load values, plots of $\sigma_{max}$ with $1/Ya^{1/2}$ were constructed as shown in Fig. 19, from which values of $K_c$ were determined and plotted as a function of $\phi_f$ as shown in Fig. 20. It is seen that $K_c$ of double-gated specimens increases with increasing $\phi_f$, with a maximum value of 2.43 MPa m$^{1/2}$ at a fibre concentration value of 15.7%. The extrapolated value of 1.26 MPa m$^{1/2}$ at $\phi_f = 0$, corresponded to the load at which the load–displacement diagram for double-gated SMA specimens deviated from linearity. It is seen also, that $K_c$ of a double-gated specimen is considerably lower than $K_c$ of a single-gated specimen.

The weldline effect is quantitatively expressed in terms of the weldline integrity parameter as shown in Fig. 21. The weldline integrity parameter for initiation was estimated to be 0.70 compared to a value 0.63 obtained by way of maximum load.

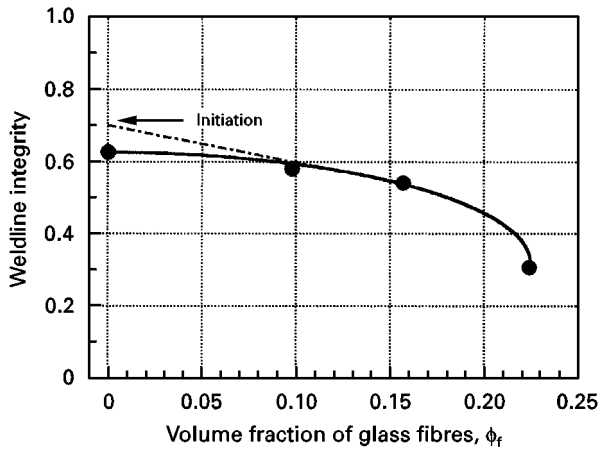


*Figure 21* Weldline integrity parameter for fracture toughness versus volume fraction of glass fibres.

## 4. Conclusions

The dependence of mechanical and fracture properties of SMA on volume fraction of glass fibres was investigated with special attention being given to the rule-of-mixtures in describing the observed variations in the measured quantities as a function of the volume fraction of the glass fibres. Results indicated that the addition of glass fibres

1. enhances tensile and flexural strengths of the polymer matrix. Variation for both strengths with respect to $\phi_f$ followed a simple rule-of-mixtures. It was found that although strengths were greater in flexure than in tension, the relative strength in each case was independent of the loading mode. Moreover, tensile strength of the polymer matrix and its composites was considerably reduced in the presence of the weldline. The weldline integrity parameter decreased linearly from a value of 0.66 for the matrix to a value of 0.25 for composite containing 22% by volume glass fibres;

2. enhances the elastic modulus of the polymer matrix. Elastic modulus was found to be independent of the loading mode, increasing linearly with increasing $\phi_f$ according to a simple rule-of-mixtures. The presence of the weldline had no significant effect upon elastic modulus;

3. enhances fracture toughness of the polymer matrix. A linear relationship was found between fracture toughness and $\phi_f$. Furthermore, fracture toughness of the polymer matrix and its composites was considerably reduced in the presence of the weldline. The weldline integrity parameter decreased from a value of 0.70 for the matrix to a value of 0.3 for composite containing 22 vol % glass fibres.

## Acknowledgement

The authors thank DSM UK for the provision of the materials.

## References

1. H. L. COX, *B. J. Appl. Phys.* **3** (1952) 72.
2. A. KELLY and W. R. TYSON, *J. Mech. Phys. Solids* **6** (1965) 13.
3. K. J. DIN and S. HASHEMI, *J. Mater. Sci.* **32** (1997) 375.
4. M. R. PIGGOTT, M. KO and H. Y. CHUANG, *Compos. Sci. Technol.* **48** (1993) 291.
5. M. R. PIGGOTT, *J. Compos. Mater.* **28** (1994) 588.
6. S. HASHEMI, M. T. GILBRIDE and J. M. HODGKINSON, *J. Mater. Sci.* **31** (1996) 5017.
7. Z. U. NABI and S. HASHEMI, *ibid.* **33** (1998) 2985–3000.
8. A. CHRYSOSTOMOU and S. HASHEMI, *ibid.* (1998) in press.
9. H. KRENCHEL, *Akad. Forlag. Copenhagen* (1964).
10. W. F. BROWN and J. E. SRAWLEY, *ASTP STP 410* (American Society for Testing and Materials, Philadelphia, PA, 1996).
11. D. O. HARRIS, *J. Bas. Eng.* **49** (1967) 89.

*Received 21 April*
*and accepted 15 May 1998*